STATE OF THE CLIMATE IN 2014

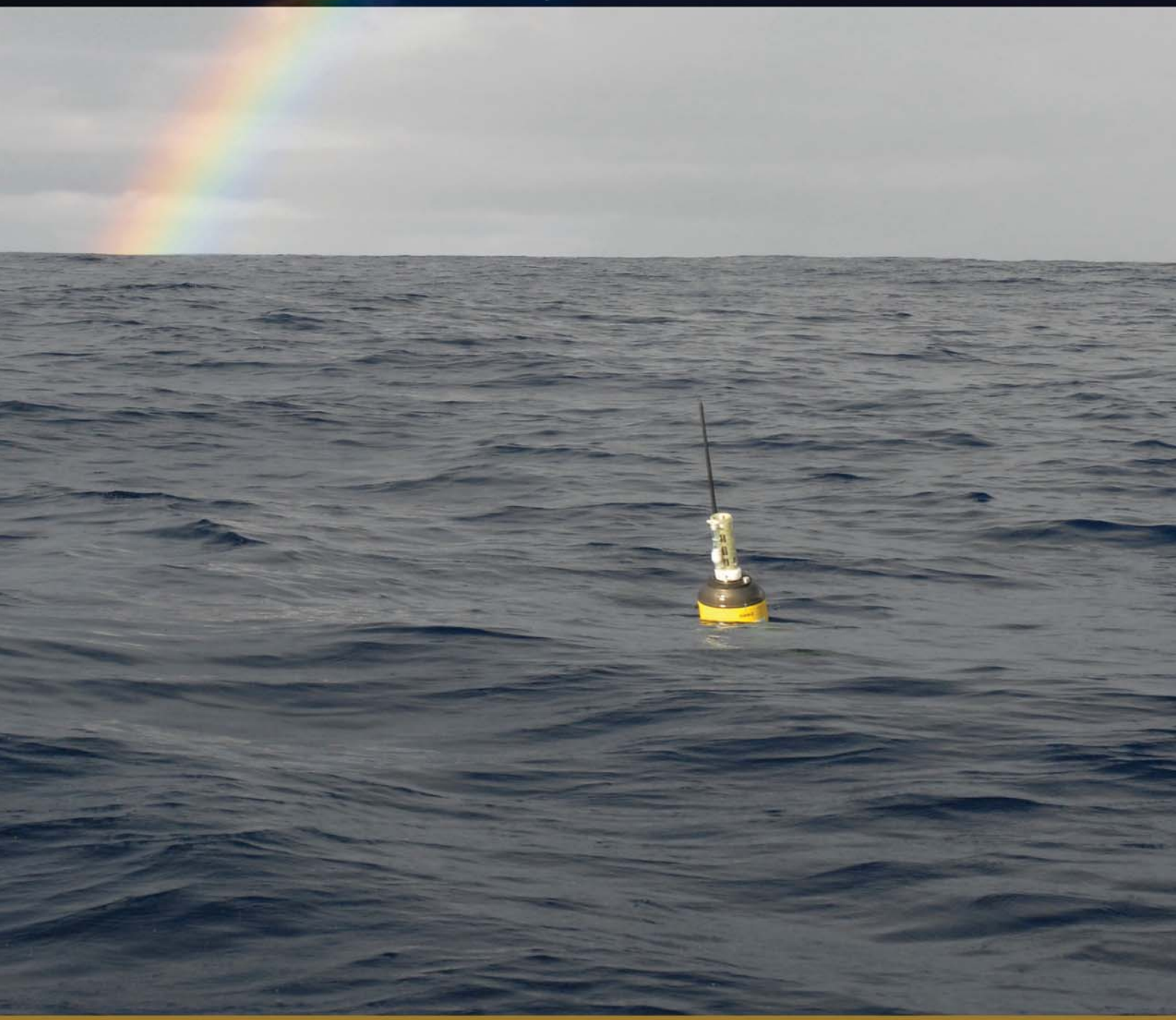

Special Supplement to the
Bulletin of the American Meteorological Society
Vol. 96, No. 7, July 2015

h. Atlantic warm pool—C. Wang

The Atlantic warm pool (AWP), defined by water warmer than 28.5°C, consists of the Gulf of Mexico, the Caribbean Sea, and the western tropical North Atlantic (Wang and Enfield 2001, 2003). The AWP is a primary moisture source for precipitation in the Americas and plays an important role in TC activity (e.g., Wang et al. 2006, 2008a, 2011; Drumond et al. 2011). Previous studies show that the AWP undergoes significant variability from seasonal to secular changes (Wang and Enfield 2003; Wang et al. 2006, 2008b). Figures 4.38a and b depict the long-term total and detrended June–November (JJASON) AWP area indices. The multidecadal and interannual variations of the AWP are displayed in Fig. 4.38c and d, respectively. The multidecadal variability (Fig. 4.38c) shows that the AWPs were larger during the period 1930–60 and since the early 2000s, and smaller during 1905–25 and 1965–95. These multidecadal variations of the AWP are consistent with the phases of the Atlantic multidecadal oscillation (AMO; Delworth and Mann 2000; Enfield et al. 2001). Because of this in-phase relationship and the importance of low-latitude heat forcing in the AWP region, the influences of the AMO on TC activity and climate may operate through the atmospheric changes induced by the AWP (Wang et al. 2008b). The JJASON AWP interannual index of Fig. 4.38d is significantly correlated with the prior December–February (DJF) Niño3 region of SST anomalies, indicating a delayed ENSO effect on the AWP (Wang et al. 2008b). Both the local oceanic/atmospheric processes and the remote delayed influence of Pacific ENSO are responsible for the interannual AWP variability.

The AWP was larger than its climatological mean each month in 2014 (Fig. 4.39a), with the largest AWP occurring in September. As shown by the climatological AWP (Fig. 4.39a), normally appears in May and peaks in September. However, the 2014 AWP appeared early in April. This is consistent with the recent study (Misra et al. 2014) which demonstrates that the onset date of the AWP during 1979–2012 ranged from late April to early August. The 2014 AWP was also distinctive in that the AWP was unusually large in November compared with the climatological AWP. As in previous years, the 2014 AWP started to develop in June between the Gulf of Mexico and Caribbean Sea with the 28.5°C SST almost overlapped with the climatological AWP (Fig. 4.39b). By July and August, the AWP was well developed in the Gulf of Mexico and Caribbean Sea and reached eastward to the western tropical North Atlantic (Fig. 4.39c,d). By September, the AWP had further expanded southeastward and the isotherm of 28.5°C covered almost the entire tropical North Atlantic (Fig. 4.39e). The AWP started to decay after October when the waters in the Gulf of Mexico began cooling (Fig. 4.39f). The isotherm of 28.5°C in November still covered the Caribbean Sea and part of the western North Atlantic Ocean (Fig. 4.39e).

C. Wang et al. (2011) has shown that AWP variability plays an important role in steering hurricanes in the Atlantic. A large AWP tends to shift the TC genesis location eastward, which increases the possibility for hurricanes to move northward without making landfall in the southeastern United States. A large AWP also weakens the North Atlantic subtropical high and produces the eastward TC steering flow anomalies along the eastern seaboard of the United States. Due to these two mechanisms, hurricanes are generally steered toward the north and northeast during a large AWP year. The TC steering flow anomalies in 2014 were consistent with those of the observed large AWP years (C. Wang et al. 2011).

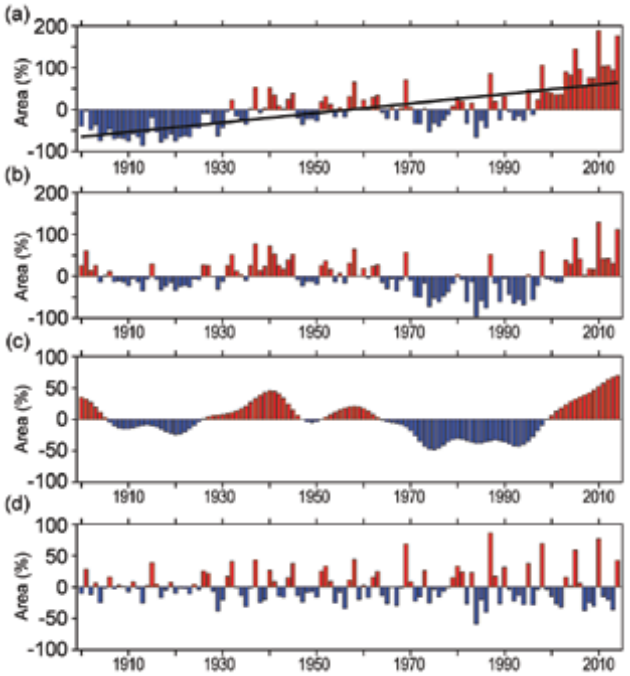

Fig. 4.38. The AWP index from 1900 to 2014. The AWP area index (% deviations from normal) is calculated as the anomalies of the area of SST warmer than 28.5°C divided by the climatological Jun–Nov AWP area. Shown are the (a) total, (b) detrended (removing the linear trend), (c) multidecadal, and (d) interannual area anomalies. The multidecadal variability is obtained by performing a 7-year running mean to the detrended AWP index. The interannual variability is calculated by subtracting the multidecadal variability from the detrended AWP index. The black straight line in (a) is the linear trend fitted to the total area anomaly. The extended reconstructed SST dataset is used.

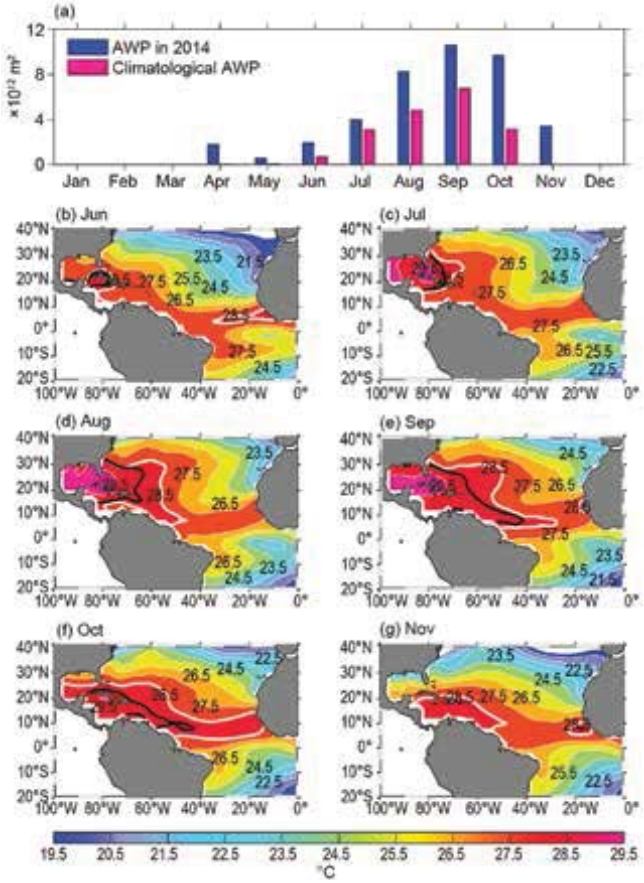

Fig. 4.39. (a) The monthly AWP area in 2014 (10^{12} m^2; blue) and the climatological AWP area (red) and the spatial distributions of the 2014 AWP in (b) Jun, (c) Jul, (d) Aug, (e) Sep, (f) Oct, and (g) Nov. The AWP is defined by SST >28.5°C. The black thick contours in (b)–(g) are the climatological AWP based on the data from 1971–2000 and the white thick contours are the 2014 28.5°C SST. The extended reconstructed SST dataset is used.

During the 2014 Atlantic tropical cyclone season of June–November, the TC steering flow anomalies were characterized by an anomalous cyclone and an anomalous anticyclone (Fig. 4.40). Associated with these patterns were the mostly eastward flow anomalies in the western tropical North Atlantic and the northward and northeastward flow anomalies in the open ocean of the North Atlantic. The distribution of the 2014 TC steering flow was unfavorable for tropical cyclones to make landfall in the southeastern United States. While a large AWP is consistent with the fact that no storms made landfall in the southeastern United States in 2014 (either by decaying or moving northward or northeastward), the AWP had no apparent enhancing effect on the number of TCs for the North Atlantic TC season [see section 4f(2)] as a large AWP typically results in more TCs (Wang et al. 2006).

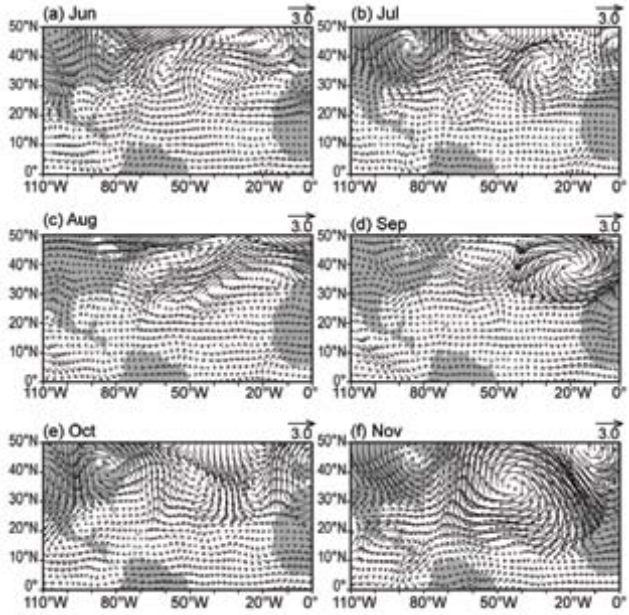

Fig. 4.40. The TC steering flow anomalies (10^3 hPa m s^{-1}) in the 2014 Atlantic hurricane season of (a) Jun, (b) Jul, (c) Aug, (d) Sep, (e) Oct, and (f) Nov. The TC steering flow anomalies are calculated by the vertically-averaged wind anomalies from 850 hPa to 200 hPa relative to the 1971–2000 climatology. The NCEP-NCAR reanalysis field is used.

i. Indian Ocean dipole—J.-J. Luo

The Indian Ocean dipole (IOD) represents a local air–sea coupled climate mode in the tropical Indian Ocean (IO). It can be driven by the tropical Pacific ENSO and/or occur independently (Luo et al. 2008, 2010). Positive IOD usually features anomalous SST cooling in the eastern IO and weak warming in the west during boreal summer and fall and vice versa for negative IOD. IOD displays a strong nonlinearity—positive IOD is usually stronger than negative IOD (Hong et al. 2008). In other words, air–sea coupling is generally weak in the negative IOD case.

Following the weak negative IOD event in 2013 (Luo 2014), SST anomalies in the tropical IO during most months of 2014 again reflected a neutral-to-weak negative IOD condition with the IOD index reaching about −0.5 in July–September 2014 (Fig. 4.41b). There are major differences between the two consecutive negative IOD events. First, the 2013 event co-occurred with a neutral-to-weak La Niña, while the 2014 event co-occurred with a neutral-to-weak El Niño condition in the Pacific (Fig. 4.41c). This suggests that this season's IOD might have been mainly driven by local processes in the IO. Second, in the 2013 case, the peak phase was generated by cold SST anomalies in the western IO and warm SST anomalies in the east during May–July 2013. Whereas, in the 2014 case, SST anomalies in both the eastern and